Hot-electron transport through thin dielectric films: Boltzmann theory and electron spectroscopy

J. Bernasconi, E. Cartier, and P. Pfluger
Asea Brown Boveri Corporate Research, CH-5405 Baden-Dättwil, Switzerland
(Received 30 December 1987; revised manuscript received 22 August 1988)

The transport problem of hot quasifree electrons through thin planar dielectric films of thickness d is considered by solving the steady-state Boltzmann equation for the electron current density $J(E,\mu,x)$, $0 \le x \le d$, within the film. The current density of injected electrons at $x=0$, $J^{(i)}(E,\mu)$, evolves to $J(E,\mu,d)$, the current density of electrons escaping the layer at $x=d$, which is calculated. In our approach, electron transport is assumed to be controlled simultaneously by energy-dependent elastic and inelastic scattering with scattering rates $\gamma^{\rm el}(E)$ and $\gamma^{\rm inel}(E)$, respectively. For inelastic scattering, one single inelastic scattering process with energy loss ΔE is assumed. With this assumption, the Boltzmann equation transforms into a set of coupled integro-differential equations which describe the cascading down of hot electrons in discrete energy steps ΔE during solid-state transport. The resulting cascade problem is then solved analytically in the two-flux approximation. The transport of zero-energy-loss electrons in the topmost energy interval ΔE at the maximum energy E_0 is considered separately. In this interval, no in-scattering from higher energies occurs and the Boltzmann equation for $J(E_0,\mu,x)$ becomes energy decoupled. An exact formal solution of the zero-energy-loss transport problem is presented and exact and approximate results for the two limiting cases of pure elastic and pure inelastic scattering are compared. Our theoretical results are then applied to typical electron transmission experiments such as internal photoemission for transport analysis (IPTA), low-energy electron transmission (LEET), and x-ray photoelectron spectroscopy (XPS) in the substrate-overlayer configuration. It is shown that energy-dependent elastic and inelastic scattering rates in wide-band-gap insulators can be extracted from IPTA and LEET experiments with our theoretical analysis. Using these results, the experimentally determined $J(E,\mu,d)$ can be reconstructed. Our analysis also allows for a rigorous definition of XPS escape lengths in terms of scattering rates.

I. INTRODUCTION

The determination of electron scattering rates (or lengths) is a crucial problem in solid-state transport of nonthermalized carriers. In particular, hot-electron transport in wide-band-gap semiconductors and insulators has attracted much attention in the last few years.[1-11] Energy-dependent scattering rates can be calculated,[4,5,7] but a full theoretical description of all relevant scattering processes and of their energy dependence is extremely involved and often not necessary for the evaluation of application-relevant quantities. In the case of SiO_2, such calculations lead to quite controversial results for the scattering rates.[4,8] In many materials of technological importance such as organic polymers, reliable calculations are at present not feasible at all.

Instead, hot-electron transport can frequently and conveniently be described with energy-dependent overall elastic and inelastic scattering rates per unit length, $\gamma^{\rm el}(E)$ and $\gamma^{\rm inel}(E)$. For example, in SiO_2 it is well established now that considerable carrier heating occurs under high-field conditions in the MV/cm range.[2] Electrons can reach a steady-state distribution with a mean kinetic energy as high as 3–6 eV without imminent destruction of the insulator. Such a behavior can be explained if the energy dependence of inelastic (LO-phonon) scattering *and* quasielastic (acoustic-phonon) scattering of hot electrons up to kinetic energies of several eV are properly included in the description of high-field transport.[3,4] Another problem of interest is dielectric breakdown in wide-band-gap insulators. Recently this phenomenon has been successfully explained in terms of the avalanche breakdown model in solids.[5,6] Within this concept the crucial material specific parameters required for the prediction of hot-electron energy distributions, electron multiplication rates, and breakdown fields are again the energy-dependent elastic and inelastic scattering rates of hot electrons up to the ionization threshold.

A direct experimental determination of energy-dependent scattering rates in wide-band-gap insulators is obviously of considerable importance and electron spectroscopy in the so-called substrate-overlayer configuration is extremely suitable for this purpose.[12] In electron spectroscopic techniques developed to probe surfaces of solids, the excited electrons are subjected to solid-state transport from the excitation site in the subsurface region before vacuum emission takes place and electron-energy distribution curves (EDC's) can be measured. In most cases, the scattering during solid-state transport is not of interest for the spectroscopists and merely complicates the interpretation of the recorded EDC's; inelastic scattering leads to loss peaks and considerable background intensities, whereas elastic scattering involving a change in particle momentum might complicate the interpretation of angle-resolved studies.[1] On the other hand, it is evident that these experiments contain useful information on solid-state transport of energetic electrons in the material under investigation. In order to extract

$\gamma^{el}(E)$ and $\gamma^{inel}(E)$ from electron spectroscopic experiments in the substrate-overlayer configuration, an adequate theoretical treatment of hot-electron transport in the conduction band of thin planar insulating films is necessary. The interpretation of the quantities which are directly obtained from the experiments (damping length, escape depth, information depth) in terms of scattering parameters (elastic and inelastic scattering rates) is not well established yet. At high energies in the keV range an important step towards a more profound interpretation of escape depths was performed by Tougaard, Sigmund, and Tofterup.[1,13] These authors showed that it is not justified in general to interpret the measured escape depth as an inelastic mean free path due to plasmon excitation. For insulators at energies below the band-gap energy (typically 10 eV), where electronic excitations are impossible and electronic transport is predominantly controlled by hot electron-phonon interaction, very little is known, both theoretically and experimentally.

The main objective of this work is to give a general description of the hot-electron transport in the conduction band of thin insulating films in terms of the (energy-dependent) elastic and inelastic scattering rates. For this purpose, we will solve the corresponding Boltzmann equation by various methods, then evaluate and compare some of our exact and approximate results for special cases. In order to obtain an analytically tractable model, we choose a fairly simple scattering probability function based on energy-dependent quasielastic scattering and energy-dependent inelastic scattering with one dominant, well-defined energy loss per inelastic scattering event. In the second part of the paper, we will apply our theoretical results to substrate-overlayer experiments in typical large-band-gap insulators such as saturated long-chain hydrocarbons[14–16] and rare-gas solids.[16–18] We do not give a detailed discussion of these recent experimental results but we intend to demonstrate the applicability of our analysis for real cases. It will be shown that our simple scattering probability function is a good description for the microscopic scattering processes in insulators at low energies where electron transport is controlled by electron-phonon interaction. The formalism will be used to extract energy-dependent elastic and inelastic scattering rates from the experimental data. Furthermore, it will be shown that the energy relaxation of hot carriers can easily be calculated within our formalism if the scattering rates are known. Finally, we will shortly comment on the interpretation of information depths extracted from x-ray photoelectron spectroscopic experiments.

II. THEORETICAL ANALYSIS

A. General description

Consider the incoherent transport of hot, quasifree electrons through a thin planar dielectric film of thickness d, let $E=\frac{1}{2}m^*v^2$ denote an electron's kinetic energy and $\mu=\cos\theta$ the cosine of the angle between its propagation direction and the positive x direction (Fig. 1). The current density of injected electrons at $x=0$, $I^{(i)}(E,\mu)$, then evolves to $I(E,\mu,d)$, the current density of electrons

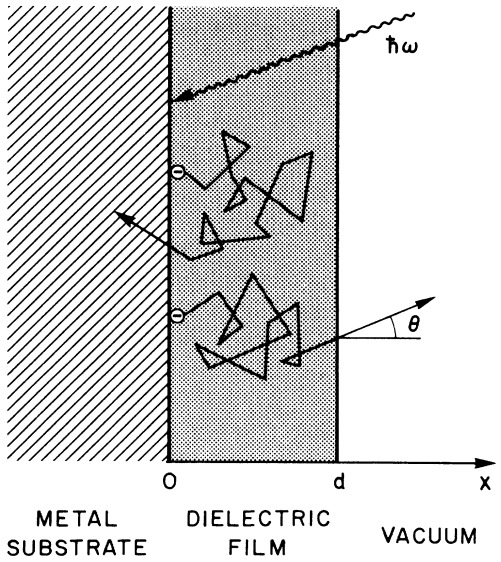

FIG. 1. Experimental geometry of substrate-overlayer experiment.

escaping the layer at $x=d$. Our aim is to express $I(E,\mu,d)$ as a function of $I^{(i)}(E,\mu)$ and of the scattering processes within the dielectric. To this end we consider the steady-state Boltzmann equation for the electron current density $I(E,\mu,x)$, $0\le x\le d$, which in the absence of an external field becomes

$$\mu\frac{\partial I(E,\mu,x)}{\partial x}=\frac{1}{2}\int_{-1}^{1}d\mu'\int_{0}^{\infty}dE'[W(\mu'\to\mu,E'\to E)I(E',\mu',x)-W(\mu\to\mu',E\to E')I(E,\mu,x)]+J^{(i)}(E,\mu)\delta(x-0^{+}), \quad (1)$$

where $W(\mu\to\mu',E\to E')$ denotes the scattering probability function and where $J^{(i)}(E,\mu)=\mu I^{(i)}(E,\mu)$ is the injected current density per unit surface area. If we assume that an electron cannot reenter once it has left the dielectric layer (either at $x=0$ or at $x=d$), the appropriate boundary conditions are

$$I(E,\mu,0)=0,\quad \mu>0 \quad (2a)$$

$$I(E,\mu,d)=0,\quad \mu<0\ . \quad (2b)$$

Equations of the type of Eq. (1) have been investigated in various contexts, e.g., in connection with radiation transfer[19,20] nonequilibrium electron distributions,[21–23] and electron-energy-loss experiments.[1,13,17,24–26] In order to obtain an analytically tractable model for the specific problem considered, most investigators have introduced a number of simplifying assumptions and approximations.

In our calculations we shall assume that the scattering processes are isotropic, and we shall further restrict ourselves to the case of a single inelastic scattering process with energy loss ΔE. The scattering probability function then becomes

$$W(\mu\to\mu', E\to E')=\gamma^{\rm el}(E)\delta(E'-E) +\gamma^{\rm inel}(E)\delta(E'-E+\Delta E) , \quad (3)$$

where $\gamma^{\rm el}(E)$ and $\gamma^{\rm inel}(E)$, respectively, denote the energy-dependent (quasi)elastic and inelastic scattering rates per unit length. The energy-loss processes occur in a discrete cascade,

$$E_k=E_0-k\,\Delta E, \quad k=0,1,2,\ldots , \quad (4)$$

where E_0 is the topmost energy of the hot electrons under consideration and k describes the number of energy-loss events. In Eq. (3), a term describing energy-gain events of the electrons is neglected, i.e., we assume low temperatures ($k_BT\ll\Delta E$). With the abbreviations

$$\gamma_k^{\rm el}\equiv\gamma^{\rm el}(E_k), \quad \gamma_k^{\rm inel}\equiv\gamma^{\rm inel}(E_k) ,$$

$$I_k(\mu,x)\equiv I(E_k,\mu,x), \quad J_k^{(i)}(\mu)\equiv J^{(i)}(E_k,\mu) ,$$

Eq. (1) is then transformed into the following set of coupled integro-differential equations:

$$\mu\frac{\partial I_k(\mu,x)}{\partial x}=-(\gamma_k^{\rm el}+\gamma_k^{\rm inel})I_k(\mu,x) +\gamma_{k\,\frac{1}{2}}^{\rm el}\int_{-1}^{1}d\mu'\,I_k(\mu',x) +\gamma_{k-1\,\frac{1}{2}}^{\rm inel}\int_{-1}^{1}d\mu'\,I_{k-1}(\mu',x) +J_k^{(i)}(\mu)\delta(x-0^+), \quad k=0,1,\ldots , \quad (5)$$

with $I_{-1}(\mu,x)\equiv 0$, and with boundary conditions

$$I_k(\mu,0)=0, \quad \mu>0 \quad (6a)$$

$$I_k(\mu,d)=0, \quad \mu<0 . \quad (6b)$$

The injection of electrons, finally, is assumed to be homogeneous over the surface $x=0$ and either isotropic or perpendicular to the film, so that

$$J_k^{(i)}(\mu)=\begin{cases}J_k^{(i)}\Theta(\mu) & \text{for isotropic injection}\\ J_k^{(i)}\delta(\mu-1) & \text{for perpendicular injection}\end{cases} \quad (7)$$

where $\Theta(\mu)$ denotes the Heaviside unit step function.

The quantities to determine are

$$J_k(\mu,d)=\mu I_k(\mu,d), \quad \mu>0 , \quad (8)$$

the current density per unit surface area of particles of energy E_k that escape the layer under a direction cosine μ, and

$$J_k(d)=\int_0^1 d\mu\,J_k(\mu,d) , \quad (9)$$

the total current density per unit surface area of particles of energy E_k escaping the layer.

B. Analysis of the zero-energy-loss electrons

In the topmost energy interval, i.e., at $E=E_0$, no in-scattering from higher energies occurs [$I_{-1}(\mu,x)\equiv 0$]. The Boltzmann equation for $I_0(\mu,x)$, Eq. (5) with $k=0$, is accordingly simplified and becomes energy decoupled:

$$\mu\frac{\partial I_0(\mu,x)}{\partial x}=-(\gamma_0^{\rm el}+\gamma_0^{\rm inel})I_0(\mu,x)+\gamma_{0\,\frac{1}{2}}^{\rm el}\int_{-1}^{1}d\mu'\,I_0(\mu',x) +J_0^{(i)}(\mu)\delta(x-0^+) . \quad (10)$$

Analytical expressions for $J_0(d)$ and $J_0(\mu,d)$ can now be obtained by different methods.

1. *Two-flux approximation*

We first discuss a simple and widely used[17,19,20,23,25,26] approximation method, originally introduced by Schuster[27] and Schwarzschild.[28] In this so-called "two-flux approximation" the angular dependence of the electronic flux is approximated by only distinguishing between a forward and a backward flux. For $I_0(\mu,x)$ we therefore write

$$I_0(\mu,x)=\begin{cases}I_0^+(x), & 0<\mu\le 1 \quad (11a)\\ I_0^-(x), & -1\le\mu<0 \quad (11b)\end{cases}$$

and integrate Eq. (10) over the appropriate μ regions. Independently of the angular distribution of the injected electrons this leads to the following two coupled linear differential equations,

$$\frac{dI_0^+}{dx}=\gamma_0^{\rm el}(I_0^- -I_0^+)-2\gamma_0^{\rm inel}I_0^+ +4J_0^{(i)}\delta(x-0^+) , \quad (12a)$$

$$\frac{dI_0^-}{dx}=\gamma_0^{\rm el}(I_0^- -I_0^+)+2\gamma_0^{\rm inel}I_0^- , \quad (12b)$$

and the boundary conditions are given by

$$I_0^+(0)=I_0^-(d)=0 . \quad (13)$$

These equations are easily solved by standard techniques, and for the current density of escaping electrons in the elastic channel (topmost energy interval) we finally obtain

$$J_0(d)=J_0^{(i)}\frac{4\gamma_0^{\rm eff}}{\Gamma_0^+\exp(2\gamma_0^{\rm eff}d)-\Gamma_0^-\exp(-2\gamma_0^{\rm eff}d)} , \quad (14)$$

where

$$\Gamma_0^{\pm}\equiv\gamma_0^{\rm el}+2\gamma_0^{\rm inel}\pm 2\gamma_0^{\rm eff} , \quad (15)$$

and

$$\gamma_0^{\rm eff}\equiv[\gamma_0^{\rm inel}(\gamma_0^{\rm inel}+\gamma_0^{\rm el})]^{1/2} . \quad (16)$$

The physical significance of the effective scattering rate $\gamma_0^{\rm eff}$ will be discussed in Sec. III. We already point out, however, that we do not in general obtain a simple exponential decay for $J_0(d)$. In the limits of very thin and very thick films we have

$$\frac{J_0(d)}{J_0^{(i)}}\cong\begin{cases}\dfrac{1}{1+(\gamma_0^{\rm el}+2\gamma_0^{\rm inel})d}, & d\ll 1/\gamma_0^{\rm eff} \quad (17a)\\ \dfrac{4\gamma_0^{\rm eff}}{\Gamma_0^+}\exp(-2\gamma_0^{\rm eff}d), & d\gg 1/\gamma_0^{\rm eff} \quad (17b)\end{cases}$$

and for two limiting cases $\gamma_0^{\text{inel}}=0$ and $\gamma_0^{\text{el}}=0$, respectively, the two-flux approximation yields

$$J_0(d)=J_0^{(i)}\frac{1}{1+\gamma_0^{\text{el}}d} \quad (\gamma_0^{\text{inel}}=0) , \tag{18}$$

and

$$J_0(d)=J_0^{(i)}\exp(-2\gamma_0^{\text{inel}}d) \quad (\gamma_0^{\text{el}}=0) . \tag{19}$$

We shall see below that the two-flux approximation predicts the behavior of $J_0(d)$ rather well. The factor of 2 in Eq. (19) arises from the integration over μ and is absent in an angular-resolved detection (see discussion in Sec. III C). The angular dependence of the escaping electrons, however, is only very crudely represented by the simple two-flux result

$$J_0(\mu,d)=2\mu J_0(d) . \tag{20}$$

Finally, we remark that the two-flux approximation can easily be extended to the case of anisotropic scattering probabilities.

2. *Method of formal integration*

An exact formal solution of the transport equation (10) is obtained by considering

$$\gamma_0^{\text{el}}\tfrac{1}{2}\int_{-1}^{1}d\mu' I_0(\mu',x)+J_0^{(i)}(\mu)\delta(x-0^+)$$

as the inhomogeneous part of an ordinary linear differential equation.[19,29] With the definition

$$\phi_0(x)\equiv\tfrac{1}{2}\int_{-1}^{1}d\mu' I_0(\mu',x) , \tag{21}$$

the formal integration of this differential equation then, in the case of isotropic injection, leads to

$$\frac{J_0(\mu,d)}{J_0^{(i)}}=\exp\left[-\frac{\gamma_0^{\text{el}}+\gamma_0^{\text{inel}}}{\mu}d\right]+\tfrac{1}{2}\gamma_0^{\text{el}}\int_0^d dx\,\phi_0(x)\exp\left[-\frac{\gamma_0^{\text{el}}+\gamma_0^{\text{inel}}}{\mu}(d-x)\right] \tag{22}$$

and

$$\frac{J_0(d)}{J_0^{(i)}}=E_2((\gamma_0^{\text{el}}+\gamma_0^{\text{inel}})d)+\frac{\gamma_0^{\text{el}}}{2}\int_0^d dx\,\phi_0(x)E_2((\gamma_0^{\text{el}}+\gamma_0^{\text{inel}})(d-x)) , \tag{23}$$

where $\phi_0(x)$ is determined by the integral equation

$$\phi_0(x)=E_1((\gamma_0^{\text{el}}+\gamma_0^{\text{inel}})x)\Theta(x-0^+)+\frac{\gamma_0^{\text{el}}}{2}\int_0^d dx'\phi_0(x')E_1((\gamma_0^{\text{el}}+\gamma_0^{\text{inel}})|x-x'|) , \tag{24}$$

and where $E_n(z)$ denotes the exponential integral

$$E_n(z)=\int_1^\infty dt\frac{e^{-zt}}{t^n} . \tag{25}$$

Our transport problem is now reduced to the solution of the integral equation for $\phi_0(x)$, Eq. (24). In the case $\gamma_0^{\text{el}}=0$ (inelastic scattering only), this is of course not necessary, and Eqs. (22) and (23) immediately reduce to the exact results

$$J_0(\mu,d)=J_0^{(i)}\exp(-\gamma_0^{\text{inel}}d/\mu) \tag{26a}$$

and

$$J_0(d)=J_0^{(i)}E_2(\gamma_0^{\text{inel}}d) . \tag{26b}$$

Except for an asymptotic expansion in the limit of very thin films, however, the integral equation (24) cannot be solved analytically if $\gamma_0^{\text{el}}\neq 0$. A numerical method to solve Eq. (24) has been proposed by Schneider.[30] In his direct approach, $\phi_0(x)$ and $E_1(z)$ are expanded in terms of appropriate Fourier series, and Eq. (24) then leads to a system of linear equations for the unknown Fourier coefficients of $\phi_0(x)$. The accuracy of the corresponding approximation for $\phi_0(x)$ therefore only depends on the number of Fourier coefficients that are taken into account.

An approximate analytical solution of the integral equation (24) can be obtained by approximating $E_1(z)$ in terms of exponential functions. A frequently used substitution is

$$E_1(z)\simeq 2\exp(-2z) \tag{27}$$

which transforms Eq. (24) into

$$\phi_0(x)=2\exp[-2(\gamma_0^{\text{el}}+\gamma_0^{\text{inel}})x]+\gamma_0^{\text{el}}\int_0^d dx'\phi_0(x')\exp[-2(\gamma_0^{\text{el}}+\gamma_0^{\text{inel}})|x-x'|] . \tag{28}$$

Equation (28) is easily solved and leads to

$$\phi_0(x)=2\frac{(\gamma_0^{\text{el}}+\Gamma_0^+)\exp[2\gamma_0^{\text{eff}}(d-x)]-(\gamma_0^{\text{el}}+\Gamma_0^-)\exp[-2\gamma_0^{\text{eff}}(d-x)]}{\Gamma_0^+\exp(2\gamma_0^{\text{eff}}d)-\Gamma_0^-\exp(-2\gamma_0^{\text{eff}}d)} \tag{29}$$

with $\Gamma_0^\pm$ and γ_0^{eff} as defined in Eqs. (15) and (16). The corresponding analytical approximations to $J_0(\mu,d)$ and $J_0(d)$ are then obtained by inserting Eq. (29) into Eqs. (22) and (23), respectively. As the resulting expressions become rather lengthy, we shall present them explicitly only for the limiting case $\gamma_0^{\text{inel}}=0$ for which they reduce to

$$J_0(\mu,d)=\frac{J_0^{(i)}}{1+\gamma_0^{\text{el}}d}[\mu(1+2\mu)+(1-2\mu)(1+\mu+\gamma_0^{\text{el}}d)\times\exp(-\gamma_0^{\text{el}}d/\mu)] \tag{30a}$$

and

$$J_0(d)=\frac{J_0^{(i)}}{1+\gamma_0^{el}d}\left[\tfrac{7}{6}+(1+\gamma_0^{el}d)E_2(\gamma_0^{el}d)\right.$$
$$\left.-(1+2\gamma_0^{el}d)E_3(\gamma_0^{el}d)-2E_4(\gamma_0^{el}d)\right] . \quad (30b)$$

If $E_2(z)$ in Eq. (23) is approximated by $\exp(-2z)$, which is consistent with Eq. (27), then Eqs. (23) and (29) lead to the same expression for $J_0(d)$ as the two-flux approximation, Eq. (14). We note, however, that for different angular distributions of the injected electrons the method of formal integration yields different expressions for $J_0(d)$ and $J_0(\mu,d)$, in contrast to the two-flux approximation.

3. *Numerical evaluation of exact and approximate results*

In the following, we evaluate and compare some of our exact and approximate results for the two limiting cases $\gamma_0^{el}=0$ and $\gamma_0^{inel}=0$. In the case $\gamma_0^{inel}=0$ we shall also compare our results with Monte Carlo simulations. The quantities we shall consider are the angularly resolved current density, $J_0(\mu,d)$, the total current density, $J_0(d)$, and the average direction cosine,

$$\langle\mu\rangle_0(d)=\frac{\int_0^1 d\mu\,\mu J_0(\mu,d)}{\int_0^1 d\mu\,J_0(\mu,d)} , \quad (31)$$

of the escaping electrons in the topmost interval $k=0$.

The quantities $J_0(d)$ and $\langle\mu\rangle_0(d)$ are plotted in Figs. 2 and 3 versus the normalized film thickness $\gamma_0^{el}d$ for purely elastic scattering ($\gamma_0^{inel}=0$). Figures 4 and 5 show the angle dependence of $J_0(\mu,d)$ for $\gamma_0^{el}=0$ and $\gamma_0^{inel}=0$, respectively. The simple two-flux approximation leads to reasonably accurate results for the total current density $J_0(d)$ of escaping electrons in both limiting cases, $\gamma_0^{inel}=0$ (Fig. 2) and $\gamma_0^{el}=0$ [where the exact result $E_2(\gamma_0^{inel}d)$ is approximated by $\exp(-2\gamma_0^{inel}d)$. It has the advantage that it can easily be generalized to more complex situations. The angle dependences, however, are only crudely represented by the two-flux approximation, and only if the thickness of the layer is not too small. The approximate evaluation of the formal integration method, on the other hand, leads to a surprisingly accurate description of $J_0(d)$ as well as of the corresponding angle distributions.

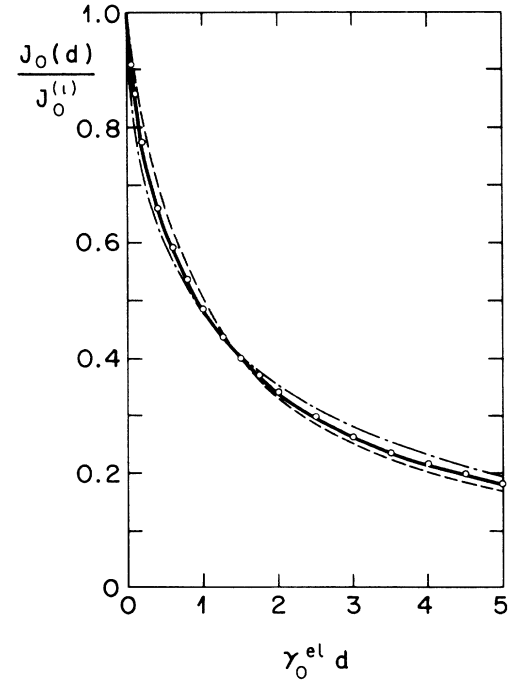

FIG. 2. Damping of the total current density J_0 as a function of normalized film thickness. Case $\gamma_0^{inel}=0$ (pure elastic scattering). Comparison of two-flux approximation (— — —) and formal integration method (exact numerical ——, and approximate —·—·— evaluation) with Monte Carlo simulations (○).

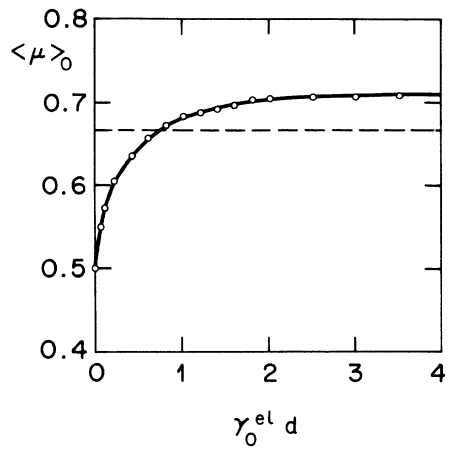

FIG. 3. Average direction cosine of the escaping electrons vs normalized film thickness. Case $\gamma_0^{inel}=0$ (pure elastic scattering). Comparison of two-flux approximation (— — —) and formal integration method (approximate evaluation, ——) with Monte Carlo simulations (○).

So far we have restricted our analysis to the fastest electrons in the topmost ($k=0$) energy interval which does not receive any intensity contribution from electrons down scattered out of higher-energy channels. In the following, we now also consider the electron current densities $J_k(d)$ in lower-energy channels ($k=1,2,\ldots$).

C. Cascade calculations

We return to our general cascade problem defined by Eqs. (5)–(7), and restrict ourselves to the two-flux approximation. This leads to a set of recursively coupled pairs of linear differential equations,

$$\frac{dI_k^+}{dx}=\gamma_k^{el}(I_k^- - I_k^+)-2\gamma_k^{inel}I_k^+ +\gamma_{k-1}^{inel}(I_{k-1}^+ + I_{k-1}^-)$$
$$+4J_k^{(i)}\delta(x-0^+) , \quad (32a)$$

$$\frac{dI_k^-}{dx}=\gamma_k^{el}(I_k^- - I_k^+)+2\gamma_k^{inel}I_k^- -\gamma_{k-1}^{inel}(I_{k-1}^+ + I_{k-1}^-) , \quad (32b)$$

with boundary conditions

$$I_k^+(0)=I_k^-(d)=0 . \quad (33)$$

A similar set of equations, with energy-independent (k-independent) scattering rates, has recently been solved by Mahan.[23] In our problem, the inelastic cascades down the energy axis can be calculated for arbitrary γ_k^{el} and γ_k^{inel}. The cascade starts at $k=0$ (with $I_{-1}^{\pm}\equiv 0$), i.e., in the topmost energy interval analyzed in the previous sub-

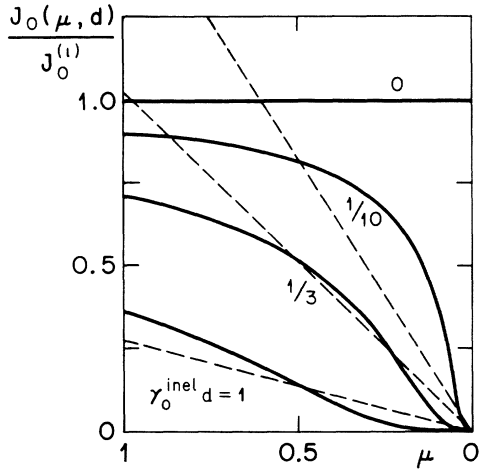

FIG. 4. Angle-resolved current density as a function of $\mu=\cos\theta$ for various film thicknesses. Case $\gamma_0^{el}=0$ (inelastic scattering only). Comparison of two-flux approximation (— — —) with the exact result, Eq. (26a) (——).

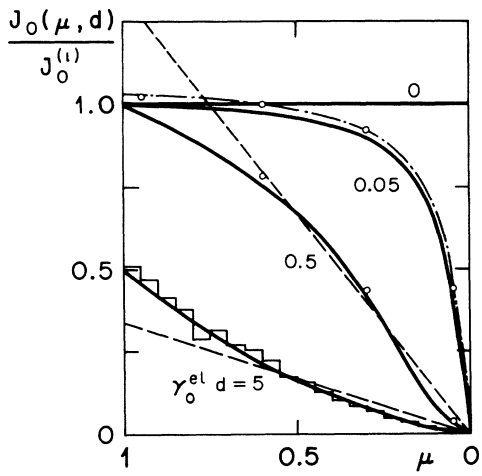

FIG. 5. Same as Fig. 4. Case $\gamma_0^{inel}=0$ (pure elastic scattering). Comparison of two-flux approximation (— — —) and formal integration method (approximate evaluation ——, exact asymptotic expansion —·—·—·) with Monte Carlo simulations (○ and histogram).

section. The bottom of the cascade ($k=K$) is reached when the electrons have been scattered inelastically until their kinetic energy E_K is lower than the characteristic energy loss ΔE (so that $\gamma_K^{inel}=0$). To solve Eqs. (32) and (33), we introduce the quantities

$$F_k(x)=\tfrac{1}{4}[I_k^+(x)+I_k^-(x)]$$

for which we obtain the recursion

$$F_k(x)=\frac{1}{S_k(d)}\left[Q_k(d-x)J_k^{(i)}+\gamma_{k-1}^{inel}\int_0^d dy\, R_k(x,y)F_{k-1}(y)\right], \tag{34}$$

where

$$S_k(x)=\Gamma_k^+\exp(2\gamma_k^{eff}x)-\Gamma_k^-\exp(-2\gamma_k^{eff}x), \tag{35a}$$

$$Q_k(x)=S_k(x)+2\gamma_k^{el}\sinh(2\gamma_k^{eff}x), \tag{35b}$$

$$R_k(x,y)=\frac{\gamma_k^{eff}}{\gamma_k^{inel}}\{\Gamma_k^+\exp[2\gamma_k^{eff}(d-|x-y|)]+\Gamma_k^-\exp[-2\gamma_k^{eff}(d-|x-y|)]-2\gamma_k^{el}\cosh[2\gamma_k^{eff}(d-x-y)]\}, \tag{35c}$$

$$\Gamma_k^{\pm}\equiv\gamma_k^{el}+2\gamma_k^{inel}\pm2\gamma_k^{eff}, \tag{35d}$$

and

$$\gamma_k^{eff}\equiv[\gamma_k^{inel}(\gamma_k^{inel}+\gamma_k^{el})]^{1/2}. \tag{35e}$$

Because of $I_k^-(d)=0$, the electron current densities $J_k(d)$ in the different channels are then simply given by

$$J_k(d)=\tfrac{1}{4}I_k^+(d)=F_k(d). \tag{36}$$

For $k=0$ [with $F_{-1}(x)\equiv0$], Eqs. (34) and (36) reduce to the explicit expression of Eq. (14) for $J_0(d)$. At least numerically, we can then successively generate the entire cascade, $J_1(d),J_2(d),\ldots,J_K(d)$, from Eqs. (34) and (36). A corresponding calculation with realistic scattering rates is presented in Sec. III.

Here we consider a simple, analytically solvable example, namely, the case of negligible elastic scattering ($\gamma_k^{el}=0$), energy-independent inelastic scattering ($\gamma_k^{inel}=\gamma$), and monochromatic electron injection ($J_k^{(i)}=J_0\delta_{k0}$). In this case, the generating function for the $F_k(x)$,

$$\Phi(t,x)=\sum_{k=0}^{\infty}t^kF_k(x),$$

can be determined explicitly:

$$\Phi(t,x)=2J_0\frac{(1+s_t)\exp[2\gamma s_t(d-x)]-(1-s_t)\exp[-2\gamma s_t(d-x)]}{(1+s_t)^2\exp[2\gamma s_t(d-x)]-(1-s_t)^2\exp[-2\gamma s_t(d-x)]}, \tag{37}$$

where

$$s_t\equiv\sqrt{1-t}. \tag{38}$$

$F_k(x)$ is then given by

$$F_k(x)=\frac{1}{k!}\frac{\partial^k\Phi(t,x)}{\partial t^k}\bigg|_{t=0}, \tag{39}$$

so that

$$J_k(d)=\frac{1}{k!}\frac{\partial^k\Phi(t,d)}{\partial t^k}\bigg|_{t=0}. \tag{40}$$

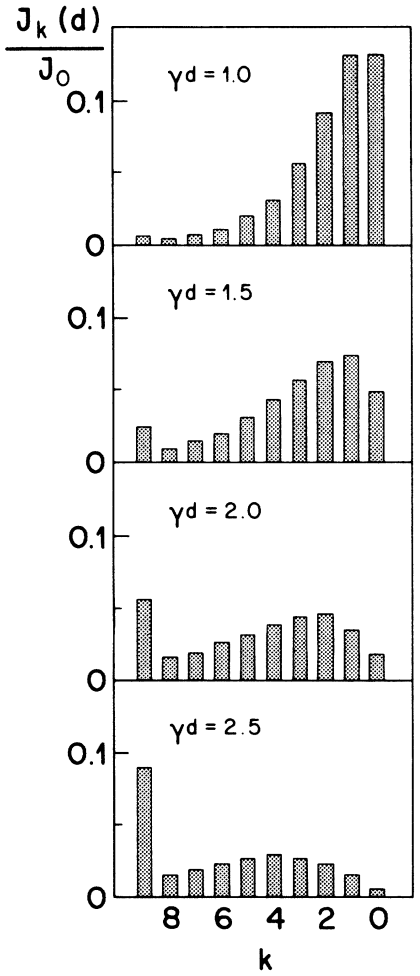

FIG. 6. Emission spectra for monochromatic electron injection at $E=E_0$, negligible elastic scattering ($\gamma_k^{el}=0$), and energy-independent inelastic scattering ($\gamma_k^{inel}=\gamma$), calculated from the cascade recursion for various normalized film thicknesses.

Equation (40) is valid for $k=0,1,\ldots,K-1$. At the bottom of the cascade ($k=K$), where γ^{inel} vanishes, we have

$$J_K(d)=\gamma\int_0^d dx\, F_{K-1}(x)\ , \tag{41}$$

where $F_{K-1}(x)$ is determined by Eqs. (39) and (37).

Corresponding emission spectra, i.e, $J_k(d)$ versus k plots, are shown in Fig. 6 for different values of the normalized film thickness γd. To generate these plots, the expressions for $F_k(x)$ and $J_k(d)$, Eqs. (39) and (40), respectively, have been evaluated with MACSYMA.

The foregoing calculations have been restricted to the case of a single energy-loss channel. If several inelastic events contribute, we may assume that they do not interfere and that a superposition of the different cascades will be observed. In particular for the case of a monochromatic injection of electrons the corresponding extensions of our calculations are straightforward. In this connection we note that an alternative way to include any number of inelastic events, the Fourier-transformation method of Michaud and Sanche,[26] can only be applied if the scattering rates are energy independent.

III. ANALYSIS OF EXPERIMENTS

In the following we will present typical experiments to which the theoretical results of Sec. II can be directly applied. As we shall see, the correct interpretation of the scattering probability function defined by Eq. (3) in terms of microscopic scattering processes in the energy range of interest is the key issue for a physical understanding of experimentally measured quantities such as the damping length or the escape depth. We will also emphasize some implications of the actual experimental boundary conditions as well as of given experimental limitations such as energy resolution or detection conditions on the applicability of our theoretical results.

A. The internal photoemission for transport analysis (IPTA) experiment

1. General description

The general situation sketched in Fig. 1 can be practically realized by internal photoemission. The principle of IPTA is shown schematically in the lower part of Fig. 7. The experiment is based on low-energy electron transmission through insulating films of various thicknesses. A broad energy distribution $J^i(E)$ of a width $w=\hbar\omega_{photon}-(E_c-E_F)$ is photoinjected at the metal-dielectric interface and the energy distribution $J(E,d)$ of vacuum emitted electrons is measured after solid-state transport. Here, E_c denotes the conduction-band edge of the insulator, and E_F is the Fermi energy of the metal. It is important to keep in mind that the injected distribution has a sharp cutoff at the maximum kinetic energy

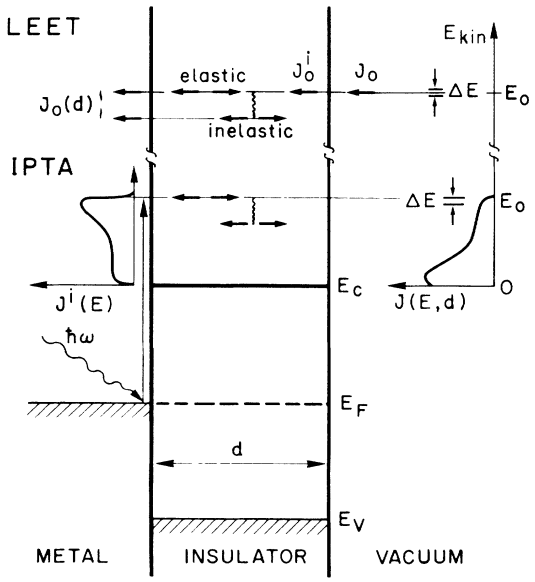

FIG. 7. Schematic comparison of the low-energy electron transmision (LEET) experiment with the method of internal photoemission for transport analysis (IPTA) in an energy-level diagram. In LEET, electrons are injected from vacuum with an electron gun and the transmitted current is collected from the metal to ground. In IPTA, electrons are injected from the metal by photoeffect and the current transmitted into vacuum is energy analyzed.

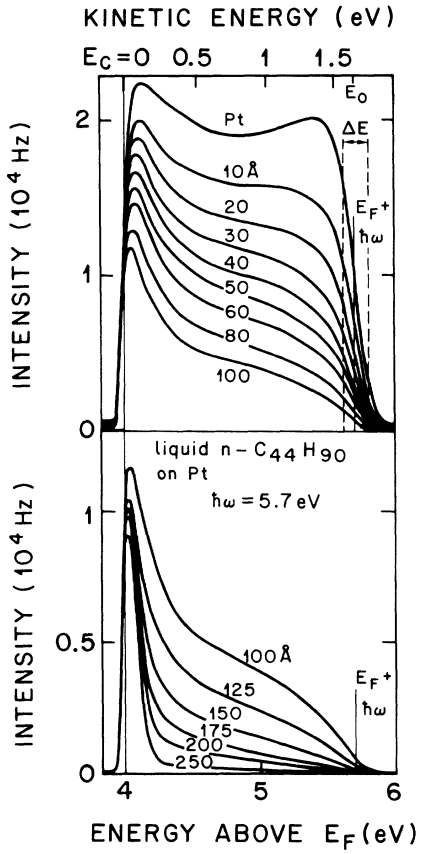

FIG. 8. Energy distributions of hot electrons after transport through liquid n-$C_{44}H_{90}$ films of various thicknesses obtained with the IPTA technique.

$E_0 = E_F + \hbar\omega - E_c$ and that E_0 can be varied via the photon energy $\hbar\omega$. The zero point of the kinetic energy scale is at the bottom of the conduction band of the insulator. In practice we use a broadband uv source in conjunction with an uv monochromator or vacuum uv lines of a rare-gas discharge lamp for injection.[15]

Figure 8 shows typical energy distribution curves (EDC's) of hot electrons escaping liquid long-chain alkane films, n-$C_{44}H_{90}$, of various thicknesses after photoinjection and solid-state transport.[31] The photon energy $\hbar\omega = 5.7$ eV yields a maximum kinetic energy $E_0 = 1.7$ eV. The scattering events during solid-state transport manifest themselves by changing the EDC's drastically as described in Sec. II. The overall intensity decreases due to electrons transported back to the metal substrate by both inelastic and elastic scattering. In addition, the spectral distribution drastically changes with thickness, the strong energy relaxation of the hot carriers being due to inelastic scattering with significant energy loss. At large thicknesses most of the carriers are completely scattered down in energy and pile up at the bottom of the conduction band. Since the electron affinity of long-chain alkanes is negative (E_0 lies above the vacuum level), carriers with energy $E \simeq k_B T$ at the bottom of the conduction band are spontaneously emitted[32,33] and the EDC of thermalized carriers can be measured. In materials with positive electron affinity conduction electrons cannot be emitted and analyzed from the region below the vacuum level, but the part of the EDC above the vacuum level can still be recorded.

2. *Topmost interval analysis*

Before using the theoretical results of Sec. II for the determination of scattering rates we first comment on the validity of a series of assumptions made in our theoretical analysis.

(1) Coherent elastic scattering in the thin overlayer films was not considered in our analysis. In principle, well-defined diffracted electron beams as in LEED (low-energy electron diffraction) can occur in transmission experiments through very thin, well-ordered films.[34] Under favorable conditions, low energy electron transmission (LEET) experiments can even be used to probe the band structure of the overlayer films.[35] In our case, however, the substrates in practice were polycrystalline and the overlayers either polycrystalline or amorphous. Furthermore, coherence is quickly lost as soon as the electrons undergo phonon collisions.[36] At $T = 300$ K, we do not expect a coherent scattering contribution to $J_0(\mu,d)$ in our experimental situations. Indeed, angle-dependent electron reflection studies did not give any indication of LEED-like spots.[33]

(2) The topmost interval ΔE at E_0 has to be defined first. In practice ΔE cannot be chosen to be smaller than the overall energy resolution $\Delta E_{\rm res}$ in the experiment which is typically 100 meV. Since the analysis of the topmost interval implies that carriers are lost from this interval of width $\Delta E \geq \Delta E_{\rm res}$ after one single inelastic scattering event, only inelastic processes with losses $\delta E^{\rm inel} > \Delta E$ are properly treated as inelastic events. On the other hand, all electrons appearing experimentally within $\Delta E_{\rm res}$ of the topmost energy E_0 are treated as elastically scattered. In reality, these electrons undergo not only pure elastic collisions, but also inelastic collisions with small losses, $\delta E \ll \Delta E_{\rm res}$. Hence, $\gamma_0^{\rm el}$ has to be considered as a quasielastic scattering rate rather than a purely elastic one. It is clear that the two rates can only be properly defined under the assumption that the scattering events can be divided into two groups according to the relation

$$\delta E^{\rm el} \ll \Delta E < \delta E^{\rm inel}, \quad \Delta E \geq \Delta E_{\rm res} . \tag{42}$$

If there are several inelastic processes which satisfy Eq. (42) all these enelastic processes will remove the carriers from the interval in one single event. $\gamma_0^{\rm inel}$ is then simply the sum of all possible inelastic scattering rates $\gamma_0^{{\rm inel},i}$, which yields

$$\gamma_0^{\rm inel} = \sum_i \gamma_0^{{\rm inel},i} . \tag{43}$$

One nice aspect of the topmost interval method is furthermore that the directional scattering characteristic which is known to be strongly energy dependent for scattering with longitudinal-optical phonons (LO phonons), for example, is irrelevant for the topmost interval

method since carriers are in any case lost from the interval after one single scattering event. The topmost interval analysis can still be used if there are several quasielastic processes which satisfy Eq. (42). In analogy to Eq. (43), the elastic scattering rate determined in the experiment is then given by

$$\gamma_0^{\mathrm{el}} = \sum_i \gamma_0^{\mathrm{el},i} . \tag{44}$$

(3) Next let us consider the validity of Eq. (42) and of our definition of the scattering probability function given by Eq. (3) for the case of saturated long-chain hydrocarbons. From high-resolution electron-energy loss studies in long-chain alkanes,[37] it is known that the dominant energy-loss processes for carriers of a few eV kinetic energy are due to excitations of molecular vibrations centered around $\delta E_1^{\mathrm{inel}} \simeq 369$ meV and $\delta E_2^{\mathrm{inel}} \simeq 160$ meV. The losses centered at $\delta E_1^{\mathrm{inel}}$ involve the stretching modes $\upsilon(CH_3)$ and $\upsilon(CH_2)$ of the alkane molecules while the loss band $\delta E_2^{\mathrm{inel}}$ is due to bending and twisting modes $\delta(CH_2)$, $\delta(CH_3)$, and $t(CH_2)$ and the C—C stretching mode. If we choose the topmost interval $\Delta E = 150$ meV, all inelastic processes discussed above satisfy Eq. (42) and γ_0^{inel} appearing in Eq. (3) has to be interpreted according to Eq. (43) as the total LO-phonon emission rate. The omission of an energy-gain term in Eq. (3) is certainly justified for the description of room-temperature experiments for which $k_B T$ is much smaller than the optical phonon energies involved in such processes. All other scattering events (deformation-potential scattering, disorder scattering, nonpolar optical phonons) are thus considered to contribute to γ_0^{el}. Hence, γ_0^{el} is again an overall quantity as defined in Eq. (44) and cannot be split into the different contributions by the experiment.

(4) As shown in Sec. II B 3, the simple two-flux approximation leads to reasonably accurate results for the total current density $J_0(d)$ of escaping electrons, whereas the angle dependences are only crudely represented. We therefore measured $J_0(d)$ instead of $J_0(d,\mu)\Delta^2\mu$, where $\Delta^2\mu$ is the aperture of the analyzer. Experimentally this can be realized by using a hemispherical retarding potential analyzer with an acceptance angle of 2π. Unfortunately, the sensitivity of the retarding potential method is fairly low since a collector current is measured instead of counting single emitted electrons. Therefore, spectra can only be taken over a limited thickness range. For these reasons we mostly used an electrostatic deflection analyzer in combination with an acceleration voltage of typically 5 V between the emitter and the analyzer entrance slit in our experiments. By this procedure a large fraction of the low-energy electrons are accelerated into the analyzer and $J_0(d)$ is reasonably well represented by the measured fraction of electrons, as can be easily checked by comparing experimental results obtained by the two techniques.

(5) The angular distribution of injected electrons does not enter in the two-flux approximation but can be expected to be somewhere between the two limiting cases given by Eq. (7). In order to determine the influence of the angular distribution, one has to go beyond the two-flux approach, using, for example, the method of formal integration discussed in Sec. II B 2. However, choosing an appropriate angular distribution for the injected distribution, $J^{(i)}(E,\mu,0)$, for real cases is by no means trivial. A good choice might actually be a cosine angular dependence which is known to be a good approximation for the angular distribution of vacuum emitted photoelectrons. We will comment on this difficulty in Sec. III C in more detail.

(6) In our analysis we neglected the (energy-dependent) electron reflection at the overlayer-metal and at the overlayer-vacuum interface. In the case of hydrocarbons with negative electron affinity, this choice is certainly justified for the overlayer-vacuum interface. For the metal-dielectric interface this choice is more questionable. Unfortunately, very little is known about electron reflection at such interfaces and the corresponding reflection coefficients at the metal-vacuum interface are frequently used instead. Within the two-flux approximation reflection coefficients can be easily included. In principle, the reflection coefficients could be treated as additional parameters which are then determined from the experiment. In practice, however, this procedure fails because the reflection coefficients and the scattering rates cannot be easily separated in the theoretical expressions [see Eqs. (45) and (47) in Sec. III B].

Within the limitations (1)–(6) discussed above, we can

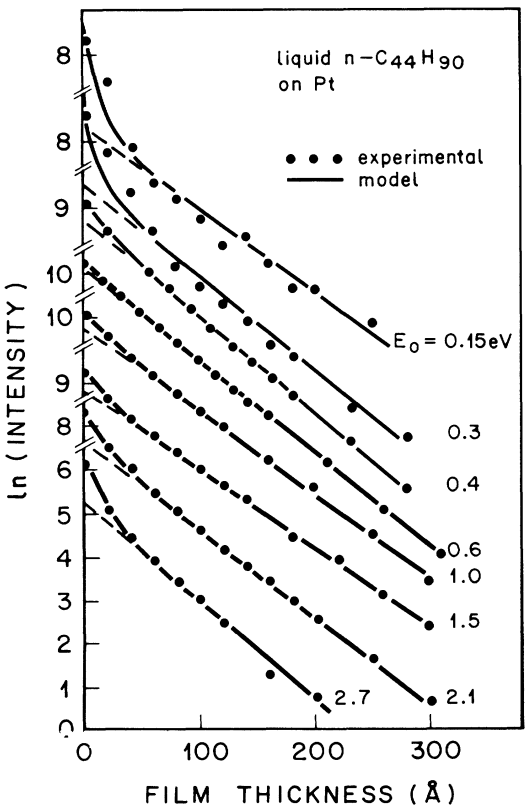

FIG. 9. Thickness dependence of the transmitted intensity $J_0(d)$ in the elastic channel (topmost interval in the IPTA experiment) measured in liquid n-$C_{44}H_{90}$ on Pt substrates. The solid lines correspond to the theoretical solution of the transport problem in the films according to Eq. (14), yielding directly the inelastic and elastic scattering rates shown in Figs. 10 and 11.

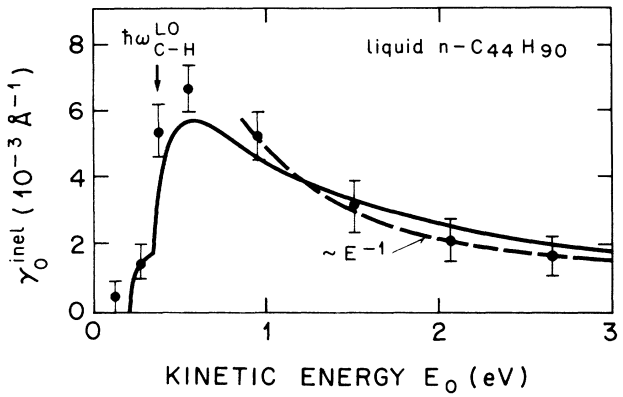

FIG. 10. Inelastic scattering rate per unit length, γ_0^{inel}, vs electron kinetic energy, E_0, in liquid n-$C_{44}H_{90}$ (Ref. 31). $\hbar\omega^{LO}_{C-H}$ indicates the energy of the dominant vibrational excitation (C-H stretching mode). The solid line shows the energy dependence of the corresponding LO phonon scattering rate calculated from optical data.

now apply the two-flux results to the topmost interval data in liquid n-$C_{44}H_{90}$. Figure 9 shows a semilogarithmic plot of the zero-energy-loss intensity versus the dielectric overlayer thickness at various energies E_0. These results were extracted from EDC's similar to those shown in Fig. 8 with $\Delta E = 150$ meV and by varying E_0 via the photon energy. We then determine γ_0^{inel} and γ_0^{el} by fitting Eq. (14) to the experimental data yielding the solid lines shown in Fig. 9. It is important to see that it is actually the deviation from an exponential damping law at small thicknesses which allows for the simultaneous determination of γ_0^{inel} and γ_0^{el}. Therefore, perfect film growth at small thicknesses is crucial for the IPTA experiment.[31] Finally, in Figs. 10 and 11 the resulting inelastic and elastic scattering rates per unit length are shown. These results are discussed in detail in a separate publication.[31] We simply mention that the results are in agreement with what is expected from electron-phonon interaction theory. This can be seen most clearly in Fig. 10. The solid line shows the LO-phonon scattering rate calculated from Fröhlich's theory for polar scattering by using experimentally determined optical constants and an effective electron mass of $2m_e$, where m_e is the free-electron mass. The strong increase of γ_0^{el} at small and large energies (Fig. 11) can be explained by disorder scattering in the liquid and by deformation-potential scattering, respectively.

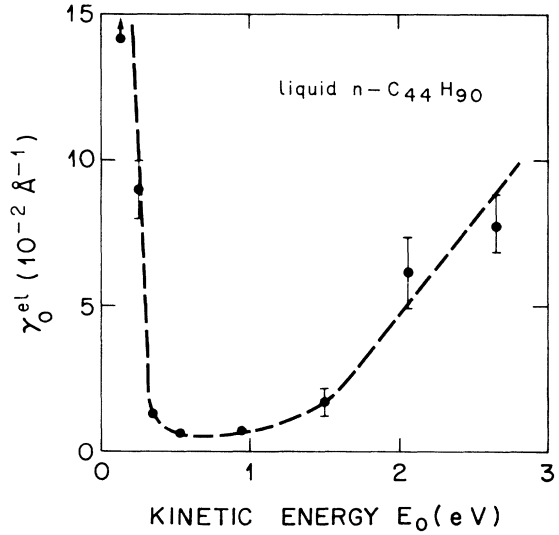

FIG. 11. Same as Fig. 10 but for the elastic scattering rate per unit path length, γ_0^{el}. The rapid increase above 1.8 eV kinetic energy is attributed to acoustic-phonon scattering, whereas the divergence at about 150 meV is attributed to the existence of a mobility edge in the liquid (disordered) state (Ref. 31).

In summary, the topmost interval analysis is a powerful tool for the experimental determination of energy-dependent elastic and inelastic scattering rates in wide-band-gap insulators. We recently applied the IPTA method to SiO_2 (Ref. 38) and obtained results which are in good agreement with scattering rates calculated by the electron-phonon interaction theory.[39]

3. *Cascade analysis technique*

In order to use the cascade formalism as actually developed in Sec. III C, we should restrict ourselves to one single well-defined energy loss only. This condition is not fulfilled in long-chain alkanes as discussed before: The total scattering cross section σ_1, for the loss modes centered around $\delta E_1^{\text{inel}} = 360$ meV, was shown to be of the same order as σ_2 (loss modes around 160 meV).[37,40] Nevertheless, to exemplify the application of the cascade analysis technique, we shall neglect the losses at δE_2^{inel} and use the recursion formulas for the electron current density in the different channels according to Eqs. (34)–(36) for the determination of scattering rates by setting $\Delta E := \delta E_1^{\text{inel}}$. This would then yield γ_k^{inel} and γ_k^{el} at many energies below E_0 from one single set of experiments as the one shown in Fig. 8, while the experiments would have to be redone at various photon energies (yielding various E_0 values) in the topmost interval approach. For $k = 0$, Eqs. (34)–(36) reduce to the topmost interval result given by Eq. (14) and yield γ_0^{el} and γ_0^{inel}. These values are then used to determine γ_1^{el} ad γ_1^{inel}, and so on. Unfortunately, the errors in γ_{k-1}^{el} and $\gamma_{k-1}^{\text{inel}}$ are progressively transferred to γ_k^{el} and γ_k^{inel}, leading to increasingly large uncertainties in the scattering rates at smaller energies.

In order to check the reliability of the $\gamma(E)$ values determined by the foregoing procedures, one may reconstruct the experimental EDC's $J(E,d)$ from the initial function $J^{(i)}(E)$ and from the scattering functions $\gamma^{\text{el}}(E)$ and $\gamma^{\text{inel}}(E)$. This constitutes a self-consistency check of our analysis method. Using the EDC of pure Pt given in Fig. 8 as a starting spectrum, we reconstructed the EDC's at larger thicknesses by using Eqs. (34)–(36) and the scattering rates shown in Figs. 10 and 11. The result is shown in Fig. 12. By comparing Fig. 12 and Fig. 8, it can be seen that the overall decrease of transmitted intensities as well as the downscattering of hot electrons are well reproduced. In order to increase the number of data points in the calculated spectra, we used two independent cascades denoted by $k = 0, 1, \ldots$ and $k = 0', 1', \ldots$. The reconstruction of the low-energy peak at small ener-

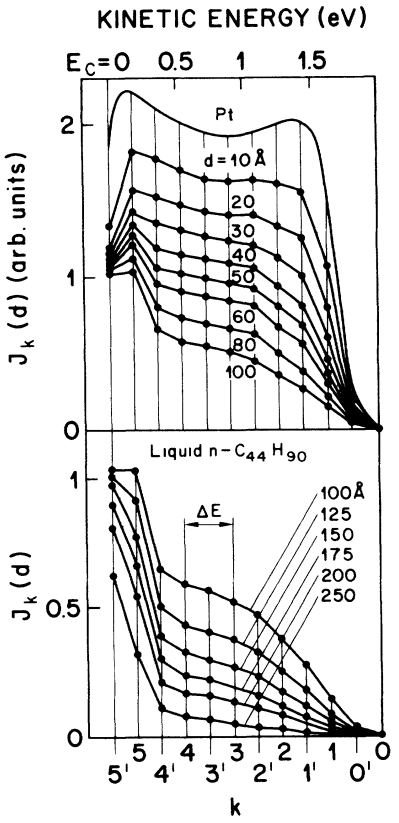

FIG. 12. Reconstruction of the IPTA spectra shown in Fig. 8 with the cascade formalism according to Eqs. (34)–(36). The scattering rates shown in Figs. 10 and 11 were used (see text).

gies depends very strongly on the divergence of γ_0^{el} at low energies, and to obtain a reasonable agreement, we had to reduce the values of γ_0^{el} below the onset of the divergence. There are many other reasons why a correct treatment of the last channels is very difficult. In our model, electrons with kinetic energy $E < \delta E_1^{inel} = 360$ meV cannot lose further energy. This, however, is not true in reality since there are other loss channels with smaller energies which are neglected in the reconstruction. In addition, low-energy electrons (≤ 500 meV) interact strongly with the trap system in real materials,[32] an effect which is not included in the presented cascade formalism.

In summary, the thickness dependence of EDC's resulting from IPTA experiments can be reconstructed (or predicted) by the cascade formalism if the energy-dependent scattering rates determined by the topmost interval method are used. This fact further supports the applicability of our analysis for IPTA experiments and confirms that reliable results for energy-dependent elastic and inelastic scattering rates can be measured in large-band-gap insulators such as long-chain alkanes (Ref. 31) and SiO_2.[38]

B. Low-energy electron transmission (LEET) experiments

Let us consider the applicability of our theory to LEET experiments. The experimental procedure is sketched in the upper part of Fig. 7. In LEET the energy E_0 of a primary electron beam with constant current density J_0 is varied and the total transmitted current $J_0(d)$ is detected. Hence, the experiment is not energy dispersive on the detection side, but rather on the injection side. It is obvious that therefore our cascade formalism cannot be used at all. In the topmost interval method there are problems as well, since the current in the interval ΔE at E_0 is detected simultaneously with the contributions at $E < E_0$ (see Fig. 7). If, however, scattering is predominantly elastic or quasielastic, the experiment is monoenergetic in the sense that the injected carriers do not leave the topmost interval ΔE at E_0 during solid-state transport. In this case we can therefore directly use our topmost interval results with $\gamma_0^{inel} = 0$ given by Eq. (18).

In practice, rare-gas solids which are nonpolar can be expected to be reasonable model substances for (quasi)elastic scattering only. In Xe, for example, the most energetic acoustic phonons have an energy of $\delta E = 6$ meV only. According to Eq. (42) we can therefore use the quasielastic approach ($\Delta E_{res} \simeq 100$ meV). We compared the LEET results in solid Xe measured by Bader *et al.*[17,18] to Eq. (18): As can be seen in Fig. 13, the inverse of the transmitted current at each energy, E_0, depends linearly on the film thickness as predicted by our theoretical result and $\gamma_0^{el}(E)$ is easily obtained from the data. For more detailed discussions of rare-gas LEET data we refer the reader to the publications of Jay-Gerin, Perluzzo, and co-workers,[9,11,17,18] and to Ref. 16. Here we only comment shortly on the influence of electron reflection at the interfaces. Let R_0^{VO}, R_0^{OM}, and R_0^{OV} be

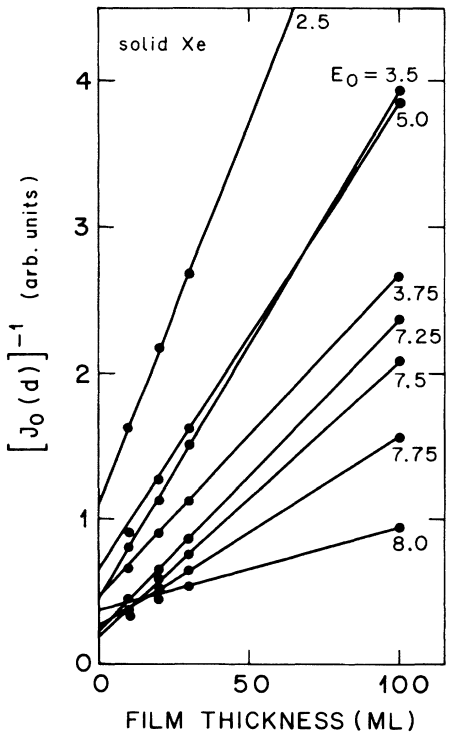

FIG. 13. Inverse of transmitted current $[J_0(d)]^{-1}$ vs overlayer thickness d in solid Xe monolayers (ML) for various electron energies, E_0, as measured in the low-energy electron transmission (LEET) experiment by Bader *et al.* (Refs. 17 and 18). $[J_0(d)]^{-1}$ varies linearly with film thickness as expected from Eq. (18), which is valid for quasielastic scattering.

the reflectivity coefficient of electrons with energy E_0 at the vacuum-overlayer, overlayer-metal, and overlayer-vacuum interfaces, respectively.

Including electron reflection for the topmost interval yields the following modified results for Eq. (18):

$$J_0(d)=J_0^{(i)}\frac{1-R_0^{\mathrm{OM}}}{1-R_0^{\mathrm{OV}}R_0^{\mathrm{OM}}+(1-R_0^{\mathrm{OV}})(1-R_0^{\mathrm{OM}})\gamma_0^{\mathrm{el}}d} \tag{45}$$

with

$$J_0^{(i)}=J_0(1-R_0^{\mathrm{VO}}) . \tag{46}$$

J_0 is the current density of the electron gun. Since the electron affinity of solid Xe is only slightly positive we may assume $R_0^{\mathrm{OV}}\simeq 0$, which leads to

$$J_0(d)=J_0^{(i)}\frac{1}{1+(1-R_0^{\mathrm{OM}})\gamma_0^{\mathrm{el}}d} . \tag{47}$$

By comparing Eq. (47) with Eq. (18) one can see that including electron reflection at the overlayer-metal interface simply leads to a rescaling of γ_0^{el} in Eq. (18) by a factor $(1-R_0^{\mathrm{OM}})^{-1}$. If R_0^{OM} is approximated by the reflection coefficient at the vacuum-metal interface R_0^{VM}, which can be measured experimentally, γ_0^{el} would be rescaled by a factor of 2.[16,18] These considerations once more demonstrate that the physics at the interfaces are important. Unfortunately, R_0^{OM} and γ_0^{el} are correlated in such a way that they cannot be separated by fitting Eq. (47) to the experimental data.

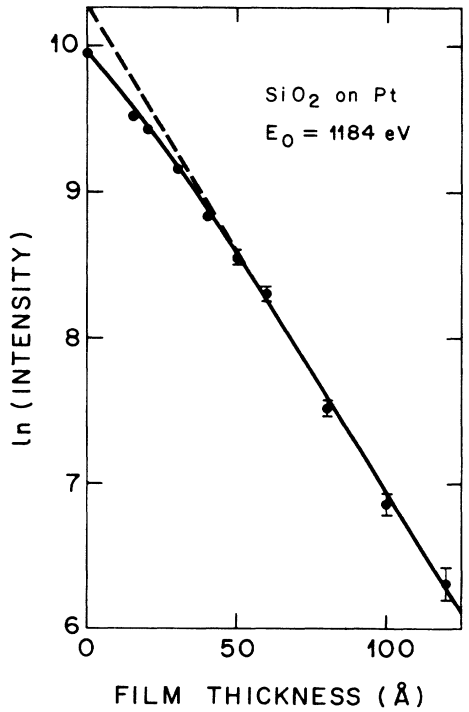

FIG. 14. Intensity of the Pt $4f_{\frac{7}{2}}$ x-ray photoelectron line (excited with Mg-$K\alpha$) vs SiO_2 overlayer thickness. The electron energy E_0 is 1184 eV in this case. The solid line was calculated by assuming forward detection, $\mu=1$, and $\gamma_0^{\mathrm{inel}}\cong\gamma_0^{\mathrm{el}}$.

C. X-ray photoelectron spectroscopy

Let us finally consider the interpretation of overlayer experiments in x-ray photoelectron spectroscopy (XPS). Usually, in these experiments the damping of a substrate core level line intensity, $J_0(d)$, at some energy E_0 is measured as a function of overlayer thickness d. The information depth (escape depth, damping length) λ_0 at energy E_0 is then usually defined by

$$J_0(d)=J_0\exp(-d/\lambda_0)\quad (d>\lambda_0) . \tag{48}$$

Equation (48) describes the experimental results rather well, but only in the thick-film limit. As an example, the damping of 1184 eV electrons through SiO_2 films is shown in Fig. 14. The interpretation of λ_0 values in terms of elastic and inelastic scattering rates attracted much attention in the last few years.[1,13,40–43] In the following, our theory will be used for that purpose and our results will be compared with earlier theoretical considerations. We restrict the discussion to the analysis of zero-loss electrons as given in Sec. II B. Again, the topmost interval has to be defined first. The natural linewidth of core level lines ΔE_c and the experimental resolution ($\Delta E_{\mathrm{res}}\cong 1$ eV) are comparable in XPS experiments. Therefore, the topmost interval cannot be chosen to be smaller than ΔE_c, which is of the order of a few eV, depending on the XPS line considered. Such a large topmost interval, $\Delta E\cong\Delta E_c$, has severe implications on the interpretation of γ_0^{inel} and γ_0^{el} given by Eqs. (43) and (44), as can be immediately seen from Eq. (42). In our example of SiO_2 overlayers on Pt (Fig. 14), the dominant LO phonon in SiO_2 has an energy of 153 meV, but $\Delta E\cong 4$ eV had to be taken to analyze the 1184 eV electrons emitted from the Pt $4f$ core level. Then, according to Eq. (42), LO phonon scattering (as well as acoustic scattering) contribute to γ_0^{el} in contrast to the IPTA experiment where they contribute to γ_0^{inel}. The major contribution to γ_0^{el}, however, in the energy range from 500 eV to a few keV results from elastic scattering by single atoms (Coulomb interaction).[42] The inelastic scattering rate γ_0^{inel} is, for XPS energies, mainly due to electronic excitations (excitons, interband transitions, plasmons) with typical losses of the order of or somewhat larger than the band-gap energy ($E_g\cong 9$ eV in SIO_2). For a more general discussion of inelastic scattering with respect to XPS energies, see, for example, Ref. 43. As shown there, plasmon excitation is the dominant inelastic process at high energies. Therefore, $(\lambda_0)^{-1}$ is often superficially interpreted as the plasmon excitation rate, while the correct interpretation of λ_0 is by no means trivial and depends on the details of the scattering physics at the energy E_0 under consideration. Particularly, it is in general not justified to identify the experimental damping lengths λ_0 as defined by Eq. (48) with the inelastic mean free path.[1,40]

In the following, we study the case of SiO_2, assuming γ_0^{el} and γ_0^{inel} to be defined according to Eqs. (42)–(44) and using the topmost interval analysis method for the interpretation of the zero-loss features in XPS experiments. If

inelastic scattering is dominant, then, and only then, Eq. (48) can be compared with Eq. (26a) for angular-resolved detection and with Eq. (26b) or Eq. (19) for angle-integrated detection. If the transmitted intensity is measured angle resolved in forward direction ($\mu=1$) this yields

$$\lambda_0=(\gamma_0^{\text{inel}})^{-1}=\lambda_0^{\text{inel}} \quad (\gamma_0^{\text{el}}\cong 0) \tag{49}$$

and for angle-integrated detection we obtain

$$\lambda_0=(2\gamma_0^{\text{inel}})^{-1}=\tfrac{1}{2}\lambda_0^{\text{inel}} \quad (\gamma_0^{\text{el}}\cong 0)\ . \tag{50}$$

If, however, elastic scattering cannot be neglected, Eq. (48) has to be compared with Eq. (17b), in the case of angle-integrated detection, which yields

$$\lambda_0=(2\gamma_0^{\text{eff}})^{-1}=\tfrac{1}{2}[\gamma^{\text{inel}}(\gamma_0^{\text{inel}}+\gamma_0^{\text{el}})]^{-1/2} \quad (d\gg 1/\gamma_0^{\text{eff}})\ . \tag{51}$$

From Eqs. (49) to (51) two important conclusions concerning the interpretation of escape depth, λ_0, in terms of scattering rates can be drawn. First, the experimental situation has to be properly taken into account. The acceptance angle of the analyzer especially is important and leads to different prefactors in the equations. Secondly only if elastic scattering can be neglected, the experimental damping law given by Eq. (48) yields directly the inelastic mean free path λ_0^{inel}. In general, λ_0 depends on both λ_0^{inel} and λ_0^{el} according to equations of the form given by Eq. (51). This has been pointed out by several authors.[1,13,40,41] Tougaard and Sigmund[13] predict nonexponential attenuation and in particular they find the attenuation to be determined by the inelastic mean-free path λ_0^{inel} at small film thicknesses and by

$$\lambda_0=\frac{1}{\sqrt{3}}(\lambda_0^{\text{inel}}\lambda_0^{\text{el}})^{1/2} \quad (d\gg\lambda_0) \tag{52}$$

at large thicknesses. Equation (52) corresponds to Eq. (51) in the limit $\gamma_0^{\text{inel}}\ll\gamma_0^{\text{el}}$ only. [The prefactor depends on the details of the model; see, for example, Eqs. (49) and (50).] The analysis of Tougaard and Sigmund is based on the assumption that the electron motion is rectilinear up to some characteristic transport time t_1, subsequently becoming and remaining diffusive. Difficulties arising from this assumption have been discussed by Dwyer and Matthew[41] by introducing elastic scattering in one-dimensional models via backscattering. They find an attenuation given by Eq. (51) with a factor $1/\sqrt{3}$ instead of $\frac{1}{2}$ which was later on confirmed by Tofterup[1] in a different treatment of the elastic scattering. For $\gamma_0^{\text{inel}}\gg\gamma_0^{\text{el}}$ Tofterup[1] obtains Eq. (26b) which is our exact result for pure inelastic scattering. If we introduce directional elastic scattering in the two-flux approximation, we obtain the same formal results as for isotropic scattering [Eqs. (14)–(19)] but with a renormalized elastic scattering rate

$$\tilde{\gamma}_0^{\text{el}}=2(1-\alpha)\gamma_0^{\text{el}}\ , \tag{53}$$

where α is the fraction of forward scattered electrons. For pure forward scattering ($\alpha=1$) $\tilde{\gamma}_0^{\text{el}}$ becomes zero as expected and the damping is exponential according to Eq. (19). For weak but pure elastic backscattering ($\alpha=0$ and $\tilde{\gamma}_0^{\text{el}}\ll\gamma_0^{\text{inel}}$) we obtain an exponential damping law again but with

$$\frac{1}{\lambda_0}=2(\gamma_0^{\text{inel}}+\gamma_0^{\text{el}}) \tag{54}$$

as previously found by Dwyer and Matthews[41] by a different approach. Equation (54) simply states that backscattering acts as an independent loss mechanism in the case of weak elastic backscattering. These comparisons show that the interpretation of λ_0 values in terms of scattering rates within the two-flux approximation in the limit $d\gg\lambda_0$ appears to be the same as the one obtained with previously considered models [apart from prefactors in Eqs. (49)–(54), which are of course important for an absolute determination of scattering rates].

Even so, the two-flux approximation has some severe drawbacks: (1) the angular distribution of the injected electrons cannot be considered in detail, (2) directional scattering can be treated in a very crude way only, and (3) the angular dependence of the emitted electrons is only crudely represented (see Sec. II B). The consequences of these limitations are most clearly seen in the thin-film limit, $d\ll\lambda_0$. For all models considered thus far in the present paper, the damping was found to be either purely exponential or stronger than exponential at small thicknesses, in contrast to the result of Tougaard and Sigmund,[13] where the damping was found to be less pronounced at small thicknesses and also in contrast to the one-dimensional models considered by Dwyer and Matthews.[41] These discrepancies are due to the different treatments of boundary conditions (detection conditions, source term in the transport problem, treatment of reflection at interfaces, etc.) and/or the different treatment of directional scattering in the different models. Dwyer and Matthews assumed the elastic scattering cross section to be pseudoisotropic with an isotropic term and a forward peaked term, whereas Tofterup used the P_1 approximation. In our two-flux approximation directional scattering was introduced by splitting γ_0^{el} into a forward scattered fraction $\alpha\gamma_0^{\text{el}}$ and a backward scattered fraction $(1-\alpha)\gamma_0^{\text{el}}$ where $\alpha\leq 1$.

The three limitations mentioned above can be overcome if the transport equation [Eq. (10)] is solved by the method of formal integration in which the various angular dependences are treated accurately. We considered some special cases in which the integration could be performed analytically by using simple approximations for the exponential integrals [see, for example, Eq. (27)]. It turns out that the damping at small thicknesses can be weaker than exponential under the following assumptions.

(1) Isotropic scattering and isotropic injection but forward detection, $\mu=1$. Forward injection enhances the effect. So does forward elastic scattering.

(2) Isotropic scattering and 2π detection but forward injection. Forward elastic scattering enhances the effect.

In addition, the ratio of $\gamma_0^{\text{inel}}/\gamma_0^{\text{el}}$ is found to be important, as one would expect. This ratio can be determined

from experimental results such as shown in Fig. 14 if the correct model is chosen. We consider case (1) above to be more appropriate for the experimental configuration in which the data shown in Fig. 14 was measured. In order to obtain the solid line shown in Fig. 14, we had to choose $\gamma_0^{\text{inel}}/\gamma_0^{\text{el}} \cong 1$ (isotropic elastic scattering was assumed). A ratio of the order of 1 is reasonable for an electron energy of 1000 eV and overlayers with low atomic numbers, confirming the results of Ref. 41 and stressing again the fact that elastic scattering cannot be neglected in the interpretation of experimental damping lengths.

In summary, the topmost interval method in the two-flux approximation yields satisfactory results for the interpretation of the escape depth λ_0 obtained from x-ray photoelectron experiments [defined by Eq. (48)]. Our results are consistent with previously published analyses. We confirm that it is not justified in general to interpret λ_0 as inelastic mean free path and that in the case of 1184 eV electrons in SiO_2 films the (quasi)elastic scattering rate is of the same order as the total inelastic scattering rate for electron-electron excitation. In the case of directional scattering the two-flux approximation still seems to hold at large film thicknesses but cannot properly reproduce the attenuation in the thin-film limit. In order to treat directional elastic scattering, the method of formal integration is more appropriate since it yields exact results for the energy-decoupled Boltzmann equation which describes the topmost interval [Eq. (10)].

IV. SUMMARY

We considered the transport of hot, quasi free electrons through thin planar films and solved the steady-state Boltzman equation by various methods. In order to obtain an analytically tractable equation we chose a simple scattering probability function which holds for isotropic elastic and inelastic scattering and one single inelastic scattering process with energy loss ΔE [Eq. (3)]. The corresponding scattering rates however, were allowed to be energy dependent. The resulting cascade problem was then solved in the two-flux approximation. We separately considered the transport of zero-energy-loss electrons (topmost interval analysis) for which the Boltzmann equation becomes energy-decoupled and can be solved exactly for special cases.

The topmost interval analysis turned out to be an extremely useful tool for the analysis of typical substrate-overlayer experiments such as internal photoemission for transport analysis (IPTA), low-energy electron transmission (LEET), and x-ray photoelectron spectroscopy (XPS) in the substrate-overlayer configuration.

We showed that the simple scattering probability function which actually allows for an analytical solution of the Boltzmann equation accounts for the microscopic scattering processes in several real cases and furthermore can be easily generalized if only the zero-energy-loss electrons are considered.

We demonstrated that energy-dependent elastic and inelastic scattering rates of hot electrons in wide-band-gap insulators can be extracted from IPTA and LEET experiments and that the escape depths derived from substrate-overlayer XPS experiments can be defined in a rigorous way in terms of elastic and inelastic energy-dependent scattering rates. The energy distribution of hot electrons traversing dielectric layers of variable thicknesses can be calculated within the cascade formalism developed in this work.

ACKNOWLEDGMENTS

We would like to thank Dr. T. Goulet, Dr. H. Dersch, Dr. H. R. Zeller, Dr. R. Marsolais, and Dr. W. R. Schneider for inspiring discussions. We are grateful to R. Weder, W. Foditsch, and F. Fiedler for excellent technical assistance in the experimets and P. Unternährer for the synthetization of high-purity n-$C_{44}H_{90}$. One of us (E.C.) is grateful to the Swiss National Science Foundation for financial support.

[1] A. L. Tofterup, Surf. Sci. **167**, 70 (1986).
[2] S. D. Brorson, D. J. DiMaria, M. V. Fischetti, F. L. Pesavento, P. M. Solomon, and D. W. Dong, J. Appl. Phys. **58**, 1302 (1985).
[3] D. J. DiMaria, M. V. Fischetti, E. Tierney, and S. D. Brorson, Phys. Rev. Lett. **56**, 1284 (1986).
[4] M. V. Fischetti and D. J. DiMaria, Phys. Rev. Lett. **55**, 2475 (1985).
[5] M. Sparks, D. L. Mills, R. Warren, T. Holstein, A. A. Mardudin, L. J. Sham, E. Loh, Jr., and D. F. King, Phys. Rev. B **24**, 3519 (1981).
[6] H. R. Zeller, P. Pfluger, and J. Bernasconi, IEEE Trans. Electron. Insul. **EI-19**, 200 (1984).
[7] G. Blatter and F. Greuter, Phys. Rev. B **34**, 8555 (1986).
[8] W. Porod and D. K. Ferry, Phys. Rev. Lett. **54**, 1189 (1985).
[9] T. Goulet, J.-P. Jay-Gerin, and J.-P. Patau, J. Electron Spectrosc. **43**, 17 (1987).
[10] H.-J. Fitting and J.-U. Friemann, Phys. Status Solidi A **69**, 349 (1982).
[11] P. Plenkiewicz, J.-P. Jay-Gerin, B. Plenkiewicz, and G. Perluzzo, Solid State Commun. **57**, 203 (1986).
[12] M. P. Seah and W. A. Dench, Surf. Interface Anal. **1**, 2 (1979).
[13] S. Tougaard and P. Sigmund, Phys. Rev. B **25**, 4452 (1982).
[14] P. Pfluger, H. R. Zeller, and J. Bernasconi, Phys. Rev. Lett. **53**, 94 (1984).
[15] E. Cartier and P. Pfluger, Phys. Rev. B **34**, 8822 (1986).
[16] E. Cartier and P. Pfluger, Phys. Scr. **T23**, 235 (1988).
[17] G. Bader, G. Perluzzo, L. G. Caron, and L. Sanche, Phys. Rev. B **26**, 6019 (1982).
[18] B. Plenkiewicz, P. Plenkiewicz, G. Perluzzo, and J.-P. Jay-Gerin, Phys. Rev. B **32**, 1253 (1985).
[19] S. Chandrasekhar, *Radiative Transfer* (Clarendon, Oxford, 1950).
[20] T. W. Tong and C. L. Tien, J. Thermal. Insul. **4**, 27 (1980).
[21] G. A. Baraff, Phys. Rev. **128**, 2507 (1962).
[22] G. A. Baraff, Phys. Rev. **133**, A26 (1964).
[23] G. D. Mahan, J. Appl. Phys. **58**, 2242 (1985); G. D. Mahan and G. S. Canright, Phys. Rev. B **35**, 4365 (1987).

[24]P. A. Wolff, Phys. Rev. **95**, 56 (1954).
[25]P. J. Chantry, A. V. Phelps, and G. J. Schulz, Phys. Rev. **152**, 81 (1966).
[26]M. Michaud and L. Sanche, Phys. Rev. B **30**, 6067 (1984).
[27]A. Schuster, Astrophys. J. **21**, 1 (1905).
[28]K. Schwarzschild, Sitzungsber. Dtsch. Akad. Wiss. Berlin, Kl. Math., Phys. Tech. **17**, 1183 (1914).
[29]J. J. Duderstadt and W. R. Martin, *Transport Theory* (Wiley, New York, 1979).
[30]W. R. Schneider (unpublished).
[31]Due to the high molecular weight of n-$C_{44}H_{90}$, liquid films are stable under UHV conditions. A detailed discussion of IPTA experiments in liquid n-$C_{44}H_{90}$ films will be given soon.
[32]E. Cartier and P. Pfluger; IEEE Trans. Electron. Insul. **El-22**, 123 (1987).
[33]M. Rei Vilar, G. Blatter, P. Pfluger, M. Heyman, and M. Schott, Europhys. Lett. **5**, 375 (1988).
[34]R. Marsolais and L. Sanche (unpublished).
[35]G. Perluzzo, G. Bader, L. G. Caron, and L. Sanche, Phys. Rev. Lett. **55**, 545 (1985).
[36]C. B. Duke and G. E. Laramore, Phys. Rev. B **2**, 4765 (1970); **2**, 4783 (1970).
[37]J. J. Pireaux, P. A. Thiry, R. Caudano, and P. Pfluger, J. Chem. Phys. **84**, 6452 (1986).
[38]E. Cartier (unpublished).
[39]M. V. Fischetti, Phys. Rev. Lett. **53**, 1755 (1984).
[40]E. Cartier, P. Pfluger, J. J. Pireaux, and M. Rei Vilar, Appl. Phys. A **44**, 43 (1987).
[41]V. M. Dwyer and J. A. D. Matthew, Surf. Sci. **143**, 57 (1984), and references therein.
[42]A. Jablonski and E. Ebel, Surf. Interface Anal. **6**, 21 (1984), and references therein.
[43]H. Ibach, in *Electron Spectroscopy for Surface Analysis*, edited by H. Ibach (Springer, Berlin, 1977), p. 1.

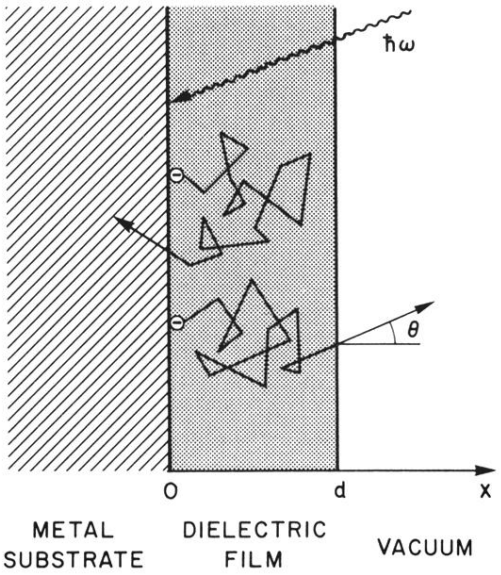

FIG. 1. Experimental geometry of substrate-overlayer experiment.

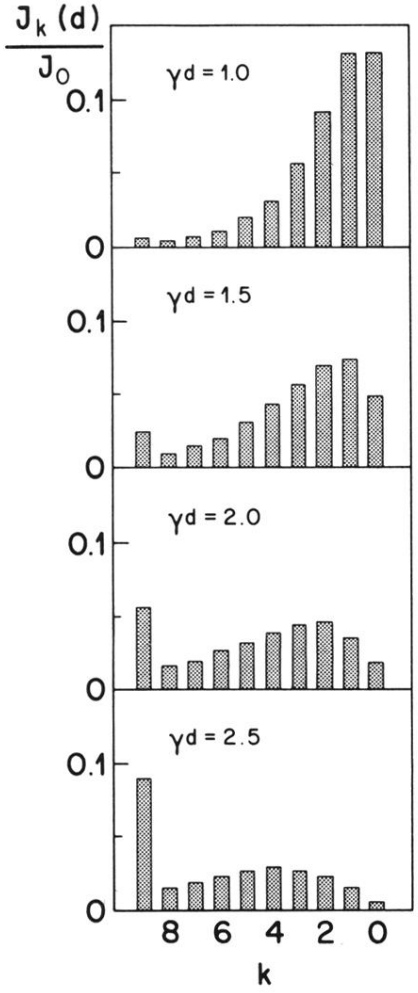

FIG. 6. Emission spectra for monochromatic electron injection at $E=E_0$, negligible elastic scattering ($\gamma_k^{el}=0$), and energy-independent inelastic scattering ($\gamma_k^{inel}=\gamma$), calculated from the cascade recursion for various normalized film thicknesses.